Infrared Physics & Technology 130 (2023) 104636

Contents lists available at ScienceDirect

Infrared Physics and Technology

journal homepage: www.elsevier.com/locate/infrared

Regular article

In situ thermal characterisation and filamentary modification in Polymethylpentene

Beining Liu [b], Xingzhu Wang [a,d,*], Juan Ahuir Torres [f], Tingyi He [g], Hongjun Zhou [c], Hong Zhao [c], Chong Zeng [c], Li Ma [e], Xihao Chen [c], Guangyu Zhu [c,*]

[a] College of Aerospace Engineering, Chongqing University, Chongqing, 400044, China
[b] School of Automation, Chongqing University, Chongqing, 402159, China
[c] School of Electronic Information and Electrical Engineering, Chongqing University of Arts and Sciences, Chongqing, 402159, China
[d] State Key Laboratory for Modification of Chemical Fibers and Polymer Materials, Donghua University, Shanghai, 200030, China
[e] National Key Laboratory of Science and Technology on Advanced Composites in Special Environments, Harbin Institute of Technology, Harbin, 150001, China
[f] General Engineering Research Institute, Faculty of Engineering and Technology, John Moores University, Liverpool, L3 3AF, UK
[g] School of Physics, Chongqing University, Chongqing, 402159, China

ARTICLE INFO

Keywords:
Femtosecond pulsed laser
Thermal measurement
PMP
NUV
IR

ABSTRACT

Polymethylpentene (PMP) polymers can be used to make advanced optics, especially for midinfrared (MIR) ultrafast optics. In this study, an optical parametric converter pumped by a Ti sapphire femtosecond laser was used to investigate the polymer. The thermal effect generated by loosely focused femtosecond near mid-infrared (MIR) pulses in bulky materials is observed in real-time, and the polymer exhibits thermal stability and conformability. To avoid strong linear absorption and to increase the nonlinear damage threshold, the spectral region for ultrafast applications is 1310 nm (0.95 eV)–1350 nm (0.92 eV). For the process in region VI, there is a sign of stronger coupling for short-wavelength photons, and the pulse duration is recommended to be lower than 160 fs. In the ultraviolet (UV) region, filamentary writing using a low-focused beam, the laser peak power was selected in the range of 2.2 MW–9.2 MW. High-density bulky gratings were written. The refractive-index modulation was significant, and the polymer exhibited highly nonlinear features. This study provides insights into the applications and production of PMP polymers in laser optics and laser engineering.

1. Introduction

Polymethylpentene (PMP) is a plastic material suitable for many applications and laser processing. The plastic commonly has very low density (ρ = 0.83 g/cm), relatively high melting point (240 °C), strong resistance to chemical corrosion, high air permeability and stable dielectric properties. This polymer can be employed to produce optical elements via injection extrusion because of its thermoplastic properties, which are suitable for large-scale production. The optical and electronic properties of PMP are attractive to various industries; therefore, this polymer has been used in many important applications [1–5]. For example, this polymer possesses a wide transmission band from the ultraviolet (UV) to the midinfrared region (MIR), and even this material has a transmission window in the far infrared region (FIR)[6]. In addition, PMPs are applied in biometric devices for ultrasound images because of their tissue-like acoustic properties of low impedance, especially for low frequency attenuation, which is ~ 81.6 $dBcm^{-1}MHz^{-1}$ [7]. Note that PMP can be built in block copolymers, in which polymer blocks are strongly bonded in a covalent method to construct a patterned chemical architecture at the nanoscale [8]. Recently, the material has the potential to make nanomaterial templates [9].

Internal inscription using ultrafast laser pulses is a powerful approach for fabricating advanced devices of diffractive optics [10], optoelectronic [11], lab-on-chip [12], micro-electro-mechanical systems (MEMS) [13], photonic crystal fibres [14], and quantum computing devices [15]. The lithography can be employed to produce similar structures with more accuracy and precise than laser inscription. The lithographic technique however requires a systematic support, increasing the cost and reducing the efficiency. Another alternative technique is to fabricate functional structures in photosensitive materials [16, 17]. Laser inscription using femtosecond pulses can directly change properties of the non-photosensitive materials [18]. The laser writing

* Corresponding authors.
E-mail addresses: wxz@cqu.edu.cn (X. Wang), zhuguangyu@cqwu.edu.cn (G. Zhu).

https://doi.org/10.1016/j.infrared.2023.104636
Received 2 September 2022; Received in revised form 18 February 2023; Accepted 28 February 2023
Available online 5 March 2023

furthermore is more feasible for operating and requires less resources. The laser writing devices at sub-nanosecond scale need high NA objectives, being the problem of the low production efficiency. This problem can be well solved using two-beam interference [19] or holographic beam splitting method [20].Using ultrafast pulses with a designated characteristic wavelength can generate functional structures in solid materials, including dielectrics [21], polymers [22] and even semiconductors [23]. This inscription opens up a method to construct 2D or 3D structures in transparent materials. The inscription can employ physical and chemical mechanisms, such as the thermomechanical effect [24], optical breakdown [25], filamentation [26], incubation [27], and photo-exciting chemical reactions [17] to conduct the inscription. The inscription can internally modify the material, producing a change in the refractive index [28]. Filamentation is a static self-guiding phenomenon which is theoretically explained by the balance between self-focusing and plasma-defocusing phenomena [29]. The focused laser beam did not diverge after passing through the focus plane owing to filamentation. This filamentation effect is a third-order nonlinear effect that leads to a considerable nonlinear absorption. The focusing fs pulse with high peak intensity creates highly localised refractive-index changes because of nonlinear absorption, resulting in multiphoton and post-ionisation. Pulse width is also an important parameter for filamentary modification [30]. The couple between the lattice temperature and electronic temperature is approximately 1 picosecond in ultrafast laser exposure. When the pulse width is less than 180 fs, the light energy can be directly coupled to the filament region, resulting in local modification. The filamentation effects can be precisely located using accurate optical energy to modify the transparent material in the bulk. Furthermore, the process has a small heat-affected zone, similar to that of the adiabatic process. In the case of a scarcely focused beam, the filamentary length can be ten times higher than the Rayleigh length [29]. By exploiting the filamentation effect, laser processing can significantly increase production. The process of concentrating a laser beam using extremely high intensity can ignite multiphoton absorption [31] and induce a permanent change in the chemical properties of polymers. For polymer materials, chemical modification can involve photoinduced or direct cleavage. It has been reported that an unsaturated carbon bond of the partial depolymerisation of m ethyl formate is produced by photoinduced cleavage [32]. PMMA experiments at NUV wavelengths suggest the direct cleavage of the polymer backbone under the formation of monomers, leading to a refractive index change.

Although the optical performance of PMP is attractive, research on polymers for ultrafast laser bulky modification is insufficient, especially on the energy deposition behaviour. In addition, the interaction of femtosecond near-mid-IR (MIR) laser pulses and polymer materials is lacking in the literature although the spectral region of MIR is defined as 2.5–5 μm wavelengths. This study investigates the nonlinear and linear absorption of femtosecond pulses with a range of wavelengths, characterising the laser-processing properties and providing precise processing parameters. The investigation of processing features can help researchers and engineers consider PMP as a new material for optical devices that work in the MIR region and ultrafast cases.

2. Experimental setup

Femtosecond laser beams with wavelengths ranging from 190 nm to 2 μm were generated using an optical parametric method. A Ti: sapphire laser was used as the pumped source. In Fig. 1(a), a retroreflector system is used to obtain super-continuum spectra. The laser beam was focused inside the sample to ignite filamentation. The laser beam with a supercontinuum signal was reflected by M2 back to the mirror (M1), which had a dielectric film coating. The reflection angle was set to approximately the Brewster angle, which acts as an attenuator. The spectral signal was collected and transmitted to an advanced-timing spectrometer. A thermal camera was used to characterise the linear absorption. Fig. 1(b) shows an optical configuration for observing the in situ thermal field. For material processing, as shown in Fig. 1(c), a Galileo telescope system was used to expand the beam to a 6-mm diameter and route it to a piece of PMP sample. Additional details are listed in Table 1.

Table 1
Experimental details.

Item	Objective/NA	λ (nm)	v(mm/s)
Thermal characterisation	singlet/0.01	1050	0
SC spectrum	singlet/0.08	387	10
Filamentary inscription	singlet/0.05–0.1	387	1
Filamentary inscription*	reflection/0.15	620–640	0.5
VBG inscription	Microscope/0.5	387	0.1

3. Results and discussions

3.1. In situ thermal characterisation

The femtosecond beam had extremely high irradiation, even for a collimated beam with a diameter of approximately 1 mm, and MIR irradiation can lead to thermal effects via laser-material interaction. The energy coupling of the interaction of the thermal effect signifies strong linear absorption. Experimental investigations are expected to provide thermal characteristics relative to linear absorption. As shown in Fig. 2, the key parameters of the femtosecond pulsed laser beam are 180 mW, 1050 nm and 170 fs for the average power, wavelength, and pulse duration, respectively. The laser beam was loosely focused using a ZnSe optical glass lens with a focal length of 150 mm. The laser beam built an infrared exposure channel in the PMP sample. The thermal graphics of this channel provide more details when linear absorption is involved. An infrared camera was used to characterise the thermophysical properties. With a camera, it is possible to obtain temperature details in the exposure channel and characterise the linear absorption. The thermographic analysis provides the time- and space-resolved evolution of temperature within the interaction zone. Therefore, an approach to the analysis of thermal evolution has become possible in principle. Fig. 2(a) shows that the ambient laboratory temperature was low. The thermal zones in each typical stage are shown in Fig. 2(b)–2(f). In the initial stage, heating is generated near the optical axes near the focused plane. The high-temperature zone then moved in the incident direction. The laser beam started to build a heat-affected zone along its propagation direction. The evolution of the heat-affected zone, as shown in Fig. 2(e) at 25 s, showed a saturated temperature T = 27.2 °C. Note that there was some off-axis low-intensity scatter from the laser beam that reached the surroundings.

Fig. 3 shows that the average temperature in the heat-affected zone varied with the exposure time. There was a steep-rising stage at the front side until 14 s, a gradually increasing stage between 14 s and 25 s. After achieving the heat equilibrium state, the increase in temperature saturates between 25 s–35 s. The temperature suddenly decreased after the cessation of laser radiation exposure, followed by a gradual decrease. In the equilibrium state, the heat-affected zone appeared spindle-shaped, as shown in Fig. 2(e), and the high-temperature region was at the front side, possibly at the focal point of the incident beam. The beam waist at the focus spot had a diameter of approximately 100 μm. Irradiation did not lead to nonlinear modification of the polymer. The saturated temperature was approximately 31.1 °C which is far below the glass-phrase transition temperature, approximately 170 °C,of PMP, suggesting that the laser pulses did not lead to permanent modification of the polymer. However, the "quasi-continuum" may begin in the energy region populated by the 300 K Boltzmann distribution [33].

Fig. 4 shows the construction of the transverse thermal zone. The profile exhibited a symmetrical shape along the optical axis, with a peak value in the middle. Significant variations were observed on both sides of the peak. Although the variation on the two sides was

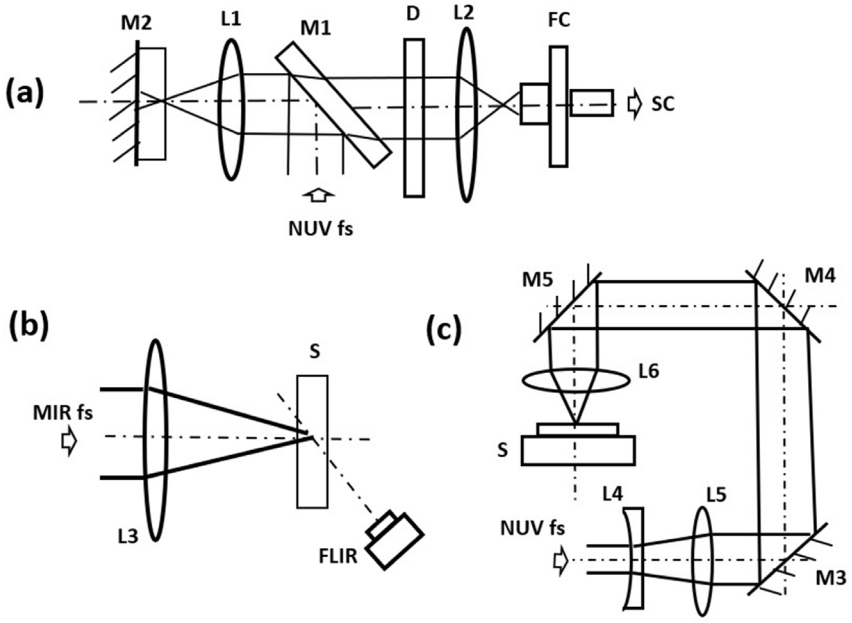

Fig. 1. Schematic setups of (a) supercontinuum spectrum analysis (b) in situ thermographic observation and (c) material processing. Lens: L1, L2, L3, L4, L5 and L6; mirrors: M1, M2, M3, M4 and M5; stage: S; density plate: D; fibre coupler: FC, supercontinuum: (SC).

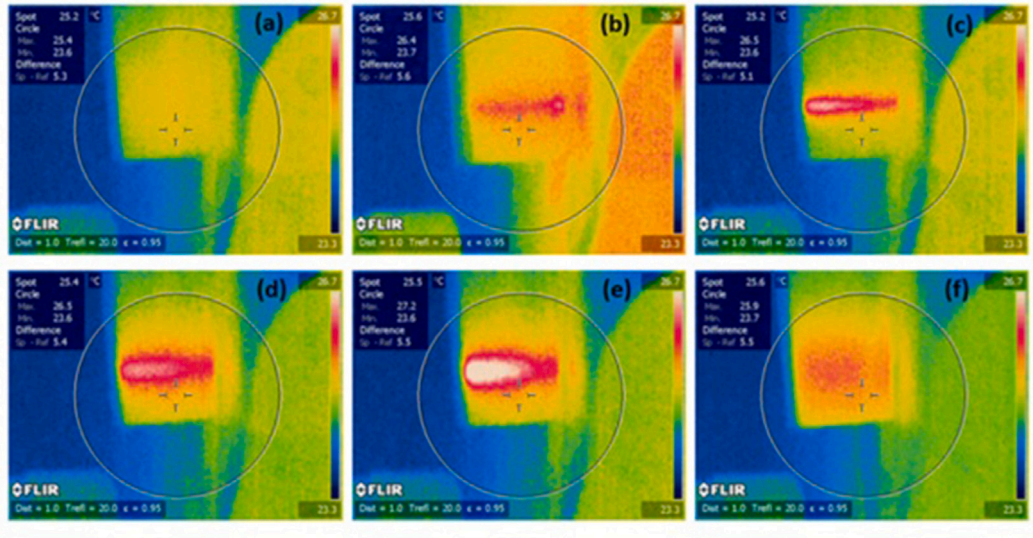

Fig. 2. Thermal effects of filamentation generated by femtosecond pulses with 1050-nm wavelength. (a) 0 s, (b) 2 s, (c) 9 s, (d) 15 s, (d) 32 s, (e) 38 s and (f) 79 s.

obvious, the peak temperatures around the symmetric axis exhibited less fluctuation. The trends displayed a significant difference from those of the Gaussian distribution.

At infrared wavelengths, interactions involve vibrational excitation, forced vibration, and the Inverse Bremsstrahlung Effect [34]. The interactions remained localised during and after the energy-coupling process. In addition, for femtosecond pulses, radiation induces electron jumping between energy levels, which is called multi-photon absorption. Bound electrons interact only weakly with the electromagnetic wave, apart from resonance; however, free electrons can be accelerated by absorbing energy from the optical e-m wave. This energy is either re-emitted or transferred to the lattice. The electric vector component of the laser radiation passing over a charged particle (electron or ion) sets the particle in motion such that a forced vibration is produced. This occurs because the frequency of the incoming radiation does not correspond to the natural resonance frequency of the lattice. The optical field can also interact with the movement of free electrons to distort the lattice by small amounts. The process of incoming photons being absorbed by electrons is known as the "Inverse Bremsstrahlung Effect".

As a supplement, an experimental study on the linear absorption of a collimated beam with a wavelength range in the near MIR region was conducted. Fig. 5 shows the coefficient of linear absorption. Absorption is considered to be the attenuation of electromagnetic waves. The polymer material dampens the intensity of the incident light at a distance, characterised by a damping constant. The intensity decays exponentially with distance from the surface to the polymer.

According to Beer Lamber law

$$I = I_0 e^{-\beta s} \tag{1}$$

where β the linear absorption coefficient. Fig. 5 shows that strong absorption occurred for photons of 1.05 eV. If PMP is used as an optical

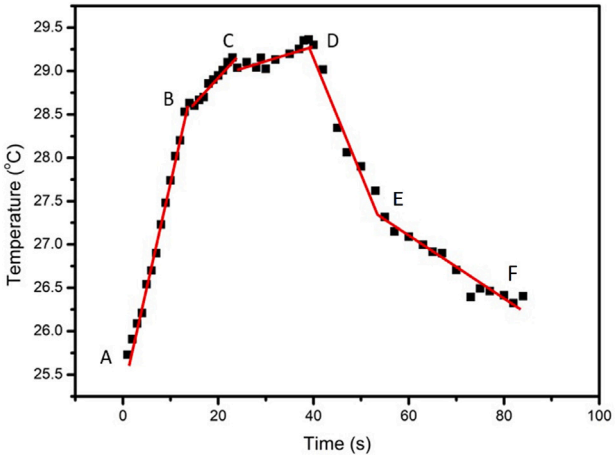

Fig. 3. Peak temperature development over time. Temperature varying: ascending stage (ABC), lumping and saturating stage (CD), descending stage (DEF).

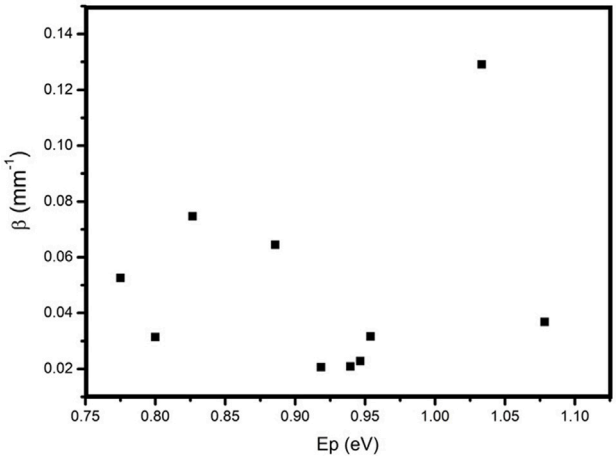

Fig. 5. The linear absorption coefficient β, corresponding to photon energy at 0.78 eV–1.78 eV of 1150 nm–1600 nm near MIR spectral region.

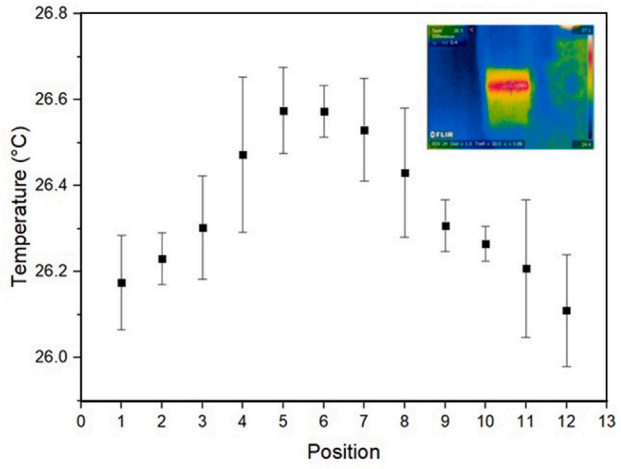

Fig. 4. Transverse thermal field.

material, the recommended region of work is 1350 nm (0.92 eV)–1310 nm (0.95 eV) to avoid strong linear absorption. In this region, the small photonic energy increases the threshold value of nonlinear damage.

These results suggested the occurrence of multiphoton infrared laser-induced processes. The forced vibration are significant, leading to extensive incubation times and significant post-pulse effects, and the energy linear coupling should be very sensitive to the pulse length. This absorption behaviour is consistent with the intramolecular redistribution of energy and is less likely to lead to unimolecular chemical reactions.

3.2. Filamentary modification

A focused laser beam with a numerical aperture (NA) of less than 0.1 was suitable for writing optical components such as waveguides. Fig. 6(a) and (b) illustrate the filamentary modification process using a convex lens with a numerical aperture of 0.05. The focusing laser beam in the sample could be seen as a light blue channel, and stray light was speculated.

Fig. 7 shows a scatter diagram of the ten groups. It can be observed that the supercontinuum (SC) spectral signal in regions I and II grew steadily, indicating the occurrence of tunnel and multiphoton ionisation [35,36], signing a gentle process. The balance between the self-focusing and defocusing effects of the plasma results in a filamentary region with uniform intensity. In addition, the filamentary process is engaged when the pulse energy exceeds the threshold value. Energy coupling is nonlinear in laser-material interaction via tunnel or multiphoton ionisation. In this nonlinear process, self-phase modulation and self-steepening broaden the laser spectrum, resulting in the SC spectrum. Filamentation has the same threshold value as SC. The spectral pattern produced by the femtosecond pulse is in terms of the anti-Stokes broadening spectrum [37]. Photonic accounts for the SC signal are collected from the region of interest (ROI), which shifts to the short-wavelength region from the fundamental wavelength of the laser. An optical circuit was set up to attain the supercontinuum spectrum (Fig. 1(a)). In region II, cascade energy coupling results from avalanche electrons which is a strong coupling process. However, the SC sample scattered for the same photo energy in each group with an obvious deviation, signifying a relatively unstable process compared to the process in region I. In region III, avalanche ionisation produces a large number of SC signals [38], signifying a fierce process. The self-focusing effect dominated the modification process. In this intermediate condition, heat is coupled to the polymer through electron heating of the lattice.

It is summarised that the thresholds for self-convergence are $p_{th0} = 2.2 \pm 0.6$ mW and $e_{th0} = 0.4 \pm 0.1$ μJ, while the thresholds for avalanche ionisation are $p_{th1} = 9.2 \pm 0.6$ MW and $e_{th1} = 1.7 \pm 0.1$ μJ which was estimated using the interpolation method. Tunnel and multiphoton absorption are the main energy-deposing methods for weak plasma formed in the region I. Photon energy plays a key role in the order of multi-photon absorption. The band gap of PMP is approximately 6.2 ev, which is the minimum excitation energy of the electronic transition from the valence band (VB) to the conduction band (CB). Therefore, ionisation was generated by two-photon coupling for 387 nm photons in the PMP. In the filamentary process, zone II was recommended, and the peak power was selected in the range of 2.2 MW–9.2 MW.

The numerical aperture (NA) plays an important role in the filamentary process [39], and NA was an effective parameter that depended on the focusing optics. When NA > 0.4, the supercontinuum phenomenon cannot be formed [38], and optical breakdown occurs. The process length of the focused Gaussian beam was calculated using Eq. (2).

$$R_L = \pi n_0 \frac{\omega_0^2}{\lambda} \tag{2}$$

In the absence of filamentation, the length produced was likely twice the Rayleigh length (RL), approximately 362 μm. Fig. 8 shows a set of filaments was processed using 387-nm (NUV) pulses femtosecond pulses with pulse energy Ep from 0.2 μ to 1.0 μJ, while transverse

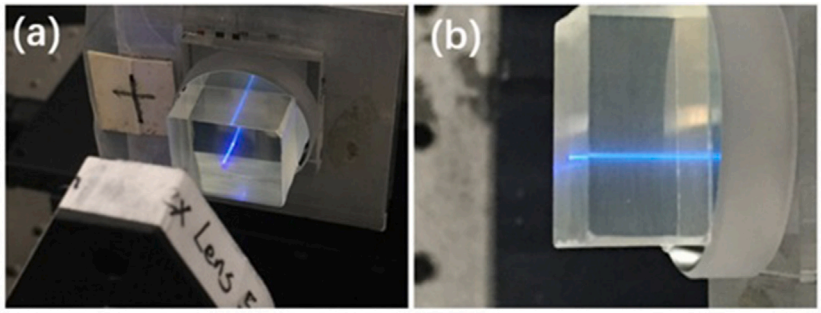

Fig. 6. (a) and (b) Processing of refractive-index modification in PMP. The laser wavelength is 387.5 nm. A singlet convex lens (focal length f = 50 mm, na 0.05) was used. The processing speed was 0.5 mm/s.

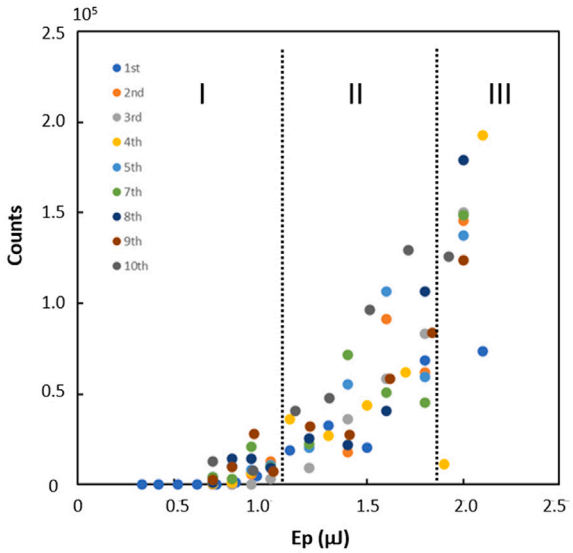

Fig. 7. Gross spectral intensity of supercontinuum versus pulse energy. I: tunnel-and-multiphoton ionisation; II: multiphoton-and-avalanche ionisation; III: avalanche ionisation.

scan speed was 1 mm/s. The maximum filament length shown was 1530 μm >> 2RL (~ 362 μm), and the shortest length was close to 2RL. The filament forming length was between 300 μm and 1500 μm, and the laser beam shown in the figure was from the right side. The starting point was located in front of the geometric focus, and this went to the light source as the energy increased [39]. This implies that the filamentation mechanism can increase the process length. The filament length had a root square relation to pulse energy, and the exponent in the experiment was approximately 0.53, which is close to the theoretical value of Zverev and Pashkov's work of 0.5 [40]. High energy can increase the filamentary length, but the process uniformity deteriorates. Fig. 9 shows the performance of the wavelength ranging from 560 nm-–640 nm. The focal point of the laser beams showed evidence of wavelength factor. The filaments responding to short wavelengths always started near the laser source, and as the wavelength increased, they receded into the material. The filaments start deeper in the material at long wavelengths. This can be explained by the higher refractive index of the material for short-wavelength light. Low coupling of photonic energy is observed, whereas stronger coupling with short-wavelength photons occurs. Furthermore, pulse duration plays a critical role in the filamentary process. There is a sign of a stronger nonlinear couple for the short-wavelength filament (top). The filamentary structure was uniform in shape and length. The pulse duration varied from 152 fs to 200 fs and the optimal duration was 152 fs. The long pulses undermine the filamentary process, leading to breakdown errors [30]. For a long-wavelength process in the region VI, the pulse duration becomes more important, and it is recommended to be lower than 160 fs.

To further understand the material modification in the filamentary region, Raman spectral analysis was performed using an Ar-ion laser with 514 nm wavelength focused via a 0.55 NA objective. Reference measurements on pristine samples show very low fluorescence and clear peaks, which is consistent with the work of Samuel and Mohan [41]. The filamentary structure was approximately 1 mm beneath the surface. The material was removed and polished for direct measurement. Compared to the analysis of the pristine PMP sample, the processed sample showed strong photoluminescence (PL) noise in the filamentary structures due to Raman scattering. If the PL signal is removed, the clean Raman peak height becomes distinct. Backbone CH stretching and CH3 asymmetric stretching contributed to peaks between 2800 and 3000 cm-1, and CH3 rocking and twisting vibrational modes contributed to peaks between 750 and 1500 cm^{-1} [42]. Fig. 10 shows the Raman spectral results with the background PL subtracted, demonstrating the decrease in the strength of all Raman peaks with increasing pulse energy. This trend suggests the existence of chemical modification mechanisms. The emergence of PL in the filament is clear and is often associated with the generation of defects and free radicals via direct laser writing [43].

3.3. The construction of bulky micro gratings

The focusing objectives with high numerical aperture (NA) are suitable for writing with precise optics. Fig. 11 shows the bulky gratings generated with laser in the sample. Fig. 12(a) shows inscription process carried out with a combinational objective with numerical aperture of approximately 0.4. The optical breakdown effects is considered for NA number is greater than 0.2 [44]. The material is directly destroyed by the optical breakdown, causing cavities and carbonisation. It is noted that the transmittance objective was formed of several optical materials. Positive Group Velocity Dispersion (GVD) can cause pulse stretch [45]. The pulse duration is a key factor for the third-order nonlinear effect called filamentation. The bulky grating specific parameter (Fig. 12(b)) were 690 μm thick, 3 μm wide, 200 lines/mm grating density and gate spacing of $\Lambda = 5$ μm. The grating sample (Fig. 12(c)) was carefully mounted on a rotating stage, permitting to bring the gratings to normal incidence prior for diffraction measurements. Detected light wavelength (Λ) value of the transmitted laser beam was 532 nm and the diffracted pattern was seen on a distant wall dim1.2 m away. The first-order diffraction efficiency at $\eta_{\pm 1}$ Bragg angle of was 39.8%, being calculated used the Eq. (3), confirming the Kogelnik theoretical fit [46]. The refractive-index modulation in the PMP was significant.

$$\eta_{\pm 1} = \sin\left(\frac{\pi \Delta n L}{\lambda \cos\theta_B}\right) \tag{3}$$

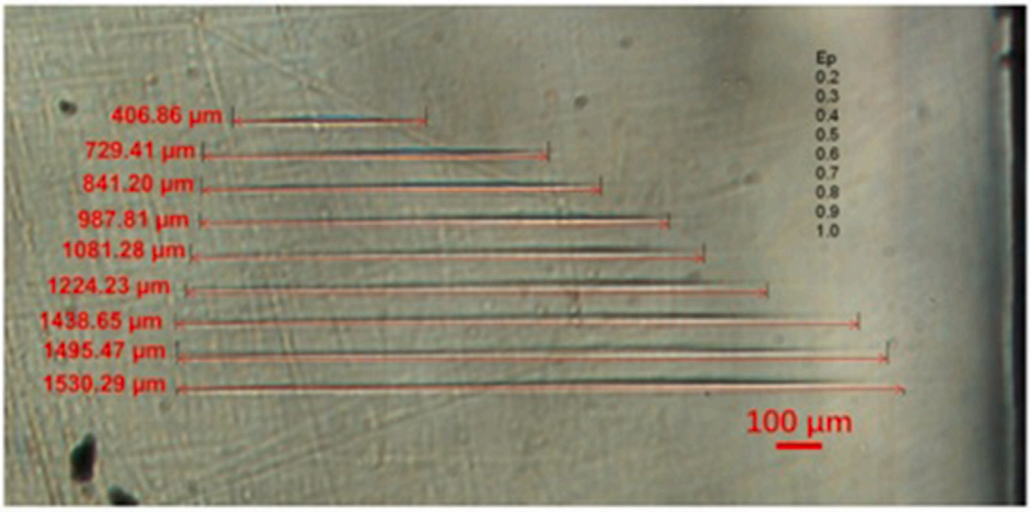

Fig. 8. Profile view of filamentary structures written by pulse energy 0.2 μJ–1.0 μJ.

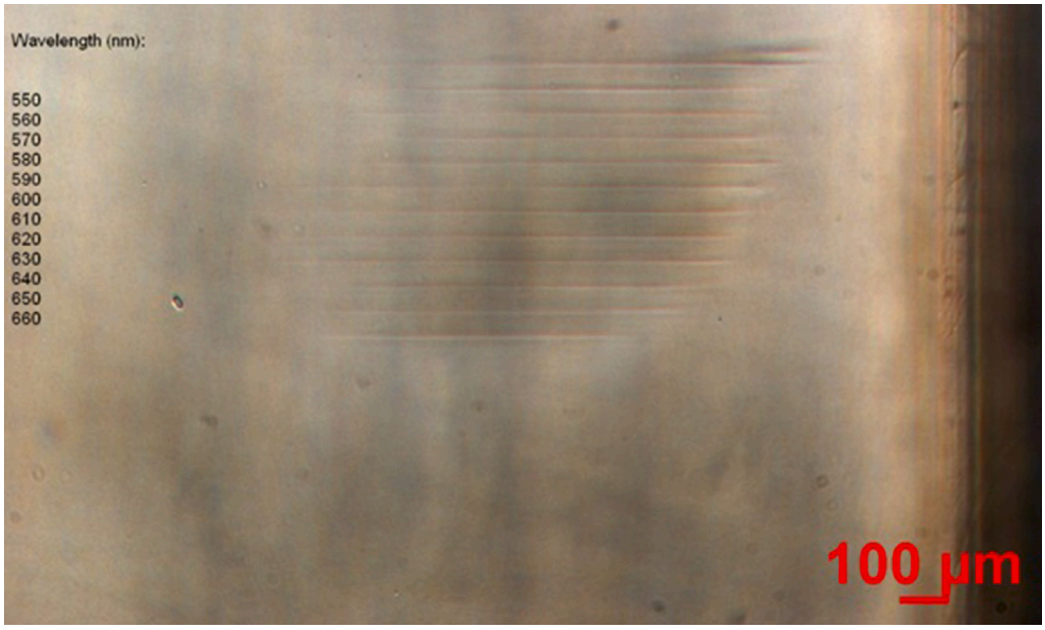

Fig. 9. Filamentary modification of wavelength ranged from 550 nm–700 nm.

Where, L is the grating thickness, Δn is the refractive index and θ_B is the Bragg angle. This result indicates a change in the refractive index to 0.01, being an order of magnitude higher than that for a lens with a small NA number. The diffraction efficiency of the gratings (Fig. 11) can be relatively low, being led by insufficient index contrast difference between modified and pristine materials. For improving diffractive efficiency, the direct approaches were increased by the thickness or line density. Using stitch-writing method can effectively be increased the thickness of the grating layer [47]. The writing of high-density gratings furthermore requires high NA objectives. The pulse duration should be lower than 160 fs for higher nonlinear effect to avoid to become a significant issue. Both approaches however lead to the problem of low production efficiency. This problem can be well solved with the usage of holographic beam splitting techniques [48].

4. Conclusions

In a study on loosely focused MIR femtosecond pulses in PMP material, the thermal effect is non-obvious and the saturated temperature is approximately 31.1 °C, which is far below the glass-phrase transition temperature, approximately 170 °C of PMP, suggesting that the laser pulses will not lead to permanent modification in the polymer. To avoid strong linear absorption, the optimised work region of PMP was 1310 nm (90.95 eV)–1350 nm (0.92 eV). In this region, smaller photonic energy increases the threshold of the nonlinear damage. For the high-throughput process of femtosecond beam, it is better to process in Zone II, and peak power is selected in the range of 2.2 MW–9.2 MW. In this region, multiphoton ionisation and avalanche ionisation are the main mechanisms to deposit energies. For NUV photons, two photons couple to form a plasma. The refractive-index modulation in the PMP is significant. For a long-wavelength process in the region VI, the pulse duration becomes more important, and it is recommended

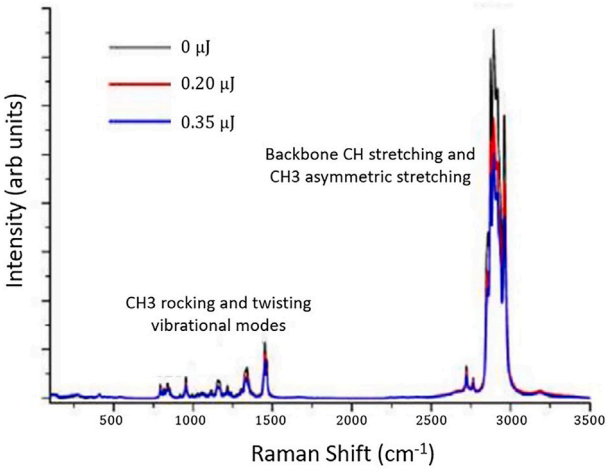

Fig. 10. The Raman spectra with background PL subtracted, suggests chemical modification mechanisms.

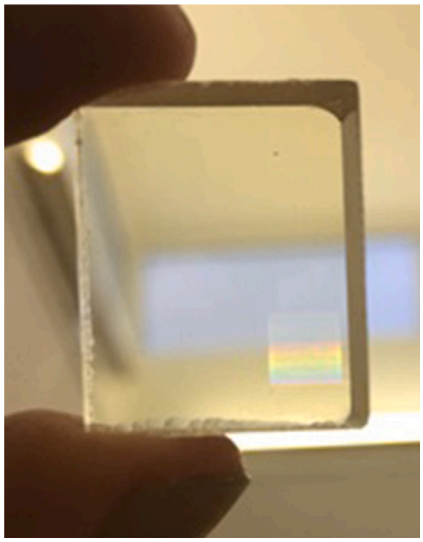

Fig. 11. Photo of 5 × 5×7 mm bulky gratings.

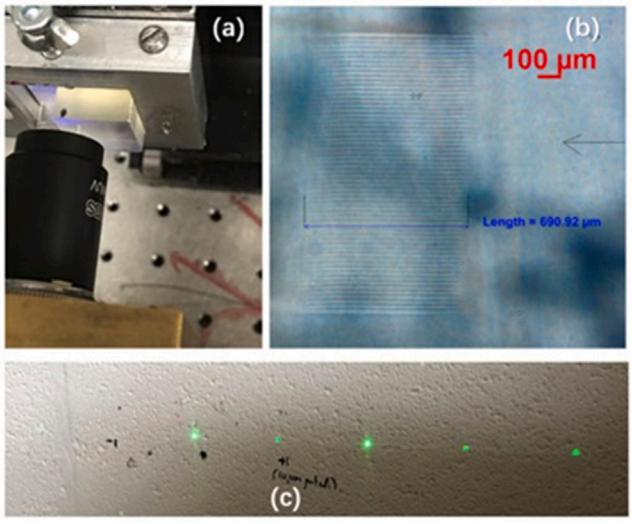

Fig. 12. (a) Internal engraving using a digital aperture of approximately 0.4 near-ultraviolet combined objective focus; (b) Side-view photomicrograph of a Bragg-like grating approximately 690 μm thick; (c) Primary diffraction test of the impaling angle incidence of a laser with a wavelength of 532 nm.

to be lower than 160 fs. Using a tightly focused beam to modify the refractive index, the change in Δn reaches 0.01, which is an order of magnitude higher than the amount of change inscribed using a lens with a small NA number.

Declaration of competing interest

The authors declare that they have no known competing financial interests or personal relationships that could have appeared to influence the work reported in this paper.

Data availability

Data will be made available on request.

Acknowledgements

This work was supported by The Science Foundation of the National Key Laboratory of Science and Technology on Advanced Composites in Special Environments (No. 6142905202711), The State Key Laboratory for Modification of Chemical Fibres and Polymer Materials (No. KF2119), The Venture and Innovation Support Program for Chongqing Overseas Returnees (No. cx2020001), The Science and Technology Research Program of Chongqing Municipal Education Commission (Grant No. KJQN202101317) and The Talent Introduction Research Funds of CQWU (Grant No. R2018SDQ13 and R2019FXCo7). The authors thank Dr. W. Perrie, Dr. S. Edwardson, and Professor G. Dearden from the University of Liverpool and Prof. L. Li from the University of Manchester for their helpful discussions and support.

References

[1] V. Golubenko, V. Gerasimova, B. Yaroslavtsev, Proton conductivity and performance in fuel cells of grafted membranes based on polymethylpentene with radiation-grafted crosslinked sulfonated polystyrene, Int. J. Hydrogen Energy (2021).
[2] R. Simone, et al., Temperature-mediated excitation of defect modes in a periodic structure at terahertz frequencies, Microw. Optical Technol. Lett. 62 (2020).
[3] B. Ghule, M. Laad, K. Tiwari, Poly-4-methyl-1-pentene a dielectric material: Patent landscape, J. Energy Storage 36 (2021) 102335.
[4] M. Matsumoto, et al., Ultrasonic evaluation of the heel fat pad under weight-bearing conditions using a polymethylpentene resin plate: Part 1, Ultrasound Med. Biol. 48 (2) (2022) 358–372.
[5] A. Mohammed, M. Ziadan, S. Al-Kabbi, Effect of donor-to-acceptor ratio on optical, electrical properties and parameters of hybrid solar cell, Int. J. Nanosci. 21 (02) (2022).
[6] D. Lytle, W. Wilkerson, G. Jaramillo, Wideband optical transmission properties of seven thermoplastics, Appl. Opt. 18 (11) (1979) 1842–1846.
[7] L. Madsen, E. Deaner, J. Mehi, Properties of phantom tissuelike polymethylpentene in the frequency range 20-70 MHZ, Ultrasound Med. Biol. 37 (8) (2011) 1327–1339.
[8] Y. Sung, et al., Syndiotactic poly (4-methyl-1-pentene)-based stereoregular diblock copolymers: Synthesis and self-assembly studies, Polymers 14 (22) (2022) 4815.
[9] S. Thangarasu, H. Oh, Impact of polymers on magnesium-based hydrogen storage systems, Polymers 14 (13) (2022) 2608.
[10] X. Zhao, et al., Long period fibre gratings inscribed by sinusoidal intensity modulated femtosecond laser, J. Optics 24 (1) (2022) 015801.
[11] P. Gotovski, et al., Inscription in the glass of efficient gauss to top-hat converters based on pancharatnam-berry phase by high power femtosecond laser pulses, in: Laser Applications in Microelectronic and Optoelectronic Manufacturing, LAMOM XXVI, 2021.
[12] A. Volpe, et al., A smart procedure for the femtosecond laser-based fabrication of a polymeric lab-on-a-chip for capturing tumor cell, Engineering (2020).
[13] T. Chen, et al., Weakening heat accumulation behavior caused by femtosecond pulses for high-performance antireflection micro-nano porous structures, Int. J. Heat Mass Transfer 164 (1) (2021) 120532.
[14] T. Allsop, et al., Long period gratings written into a photonic crystal fibre by a femtosecond laser as directional bend sensors, Optics Commun. 281 (20) (2008) 5092–5096.
[15] G. Corrielli, A. Crespi, R. Osellame, Femtosecond laser micromachining for integrated quantum photonics, Nanophotonics 10 (2021).

[16] A. Ovsianikov, A. Ostendorf, N. Chichkov, Three-dimensional photofabrication with femtosecond lasers for applications in photonics and biomedicine, Appl. Surf. Sci. 253 (15) (2007) 6599–6602.
[17] D. Bryce, et al., Characterization of a silica-pva hybrid for high density and stable silver dissolution, Mater. Chem. Phys. (2016).
[18] R. Bhardwaj, et al., Femtosecond laser-induced refractive index modification in multicomponent glasses, J. Appl. Phys. 97 (8) (2005) 107.
[19] J. Xin, L. Dong, Fabrication of complex micro/nanopatterns on semiconductors by the multi-beam interference of femtosecond laser, Physics Procedia 56 (2014) 1059–1065.
[20] G. Zhu, et al., Investigation of the thermal and optical performance of a spatial light modulator with high average power picosecond laser exposure for materials processing applications, J. Phys. D (2018).
[21] P.G.D.A. Martínez, et al., Modeling the time-dependent electron dynamics in dielectric materials induced by two-color femtosecond laser pulses: applications to material modifications, Phys. Rev. A 103 (3) (2021) 033107.
[22] Q. Li, et al., Femtosecond laser micro-structuring of amorphous polyether(Ether)ketone at 775 nm and 387 nm, J. Phys. D 53 (36) (2020) 365301, 14.
[23] A. Chimmalgi, et al., Nanostructuring of semiconductor materials and metallic thin films using femtosecond laser and scanning probe microscope, in: Commercial and Biomedical Applications of Ultrafast Lasers III Department of Mechanical Engineering, Vol. 4978, University of California, Berkeley, CA, 2003, pp. 129–137.
[24] A. Inogamov, et al., Ultrashort laser-matter interaction at moderate intensities: two-temperature relaxation, foaming of stretched melt, and freezing of evolving nanostructures, in: Fundamentals of Laser-Assisted Micro- and Nanotechnologies 2013 International Society for Optics and Photonics, 2013.
[25] M. Lenzner, et al., Femtosecond optical breakdown in dielectrics, Phys. Rev. Lett 80 (18) (1998) 4076–4079.
[26] H. Meyer, R. Alfano, Degenerate and non-degenerate conical emission and the transient Kerr nonlinear index in BK-7 glass with femtosecond laser pulses, Opt. Commun.: J. Devoted Rapid Publ. Short Contrib. Field Optics Interact. Light Matter 513- (2022) 513.
[27] B.X. Wang, et al., Rapid fabrication of smooth micro-optical components on glass by etching-assisted femtosecond laser modification, Materials 15 (2) (2022) 678.
[28] J. Zhao, et al., Review of femtosecond laser direct writing fiber-optic structures based on refractive index modification and their applications, Optics Laser Technol. 146 (2022) 107473-.
[29] A. Couairon, et al., Femtosecond filamentation in transparent media - ScienceDirect, Phys. Rep. 441 (2–4) (2007) 47–189.
[30] C. Tien, et al., Short-pulse laser damage in transparent materials as a function of pulse duration, Phys. Rev. Lett. 82 (19) (1999) 3883–3886.
[31] A. Couairon, et al., Filamentation and damage in fused silica induced by tightly focused femtosecond laser pulses, Phys. Rev. B 71 (12) (2005) 1254351–125435.11.
[32] A. Baum, et al., NUV and NIR femtosecond laser modification of PMMA, 2007.
[33] S. Molodtsov, et al., Quantum cascade laser with bound-to-quasi-continuum optical transitions at a temperature of up to 371 K, Quantum Electron. 50 (8) (2020) 710–713.
[34] Y. Kostyukov, M. Rax, Ultrahigh-intensity inverse-bremsstrahlung absorption, Phys. Rev. Lett. 83 (11) (1999) 2206–2209.
[35] A. Rudenko, et al., Single ionization of atoms in intense laser pulses: Evolution from multiphoton to tunnel ionization, Proc. SPIE - Int. Soc. Opt. Eng. 6256 (2006).
[36] Popov S., Tunnel and multiphoton ionization of atoms and ions in a strong laser field (Keldysh theory), Phys.-Usp. 47 (9) (2004) 921–951.
[37] D. Mestdagh, M. Haelterman, Spectral super-broadening of ultra-short pulses in a nonlinear kerr medium; Effect of relaxation, Opt. Commun. 61 (4) (1987) 291–295.
[38] P. Sukhorukov, Y. Vislobokov, Low- and high-frequency continuum generation by femtosecond pulses in fused silica, Quantum Electron. 37 (11) (2007) 1015.
[39] C. Richardson, et al., Femtosecond laser microstructuring and refractive index modification applied to laser and photonic devices, Proc. SPIE - Int. Soc. Opt. Eng. 5347 (2004) 18–27.
[40] M. Zverev, A. Pashkov, Self-focusing of laser radiation in solid dielectrics, Sov. Phys.—JETP 30 (1970) 616–621.
[41] E. Samuel, S. Mohan, Vibrational spectra and analysis of 2-methyl para benzoquinone, Indian J. Phys. B Proc. Indian Assoc. Cultivation Sci. B 77B (5) (2003) 575–578.
[42] Y. Song, K. Shim, Synthesis of poly(phenylene-alt-thiophene) polymer and characterization of its light emitting properties, Synth. Met. 111 (none) (2000) 437–439.
[43] J. Ashcom, Numerical aperture dependence of damage and supercontinuum generation from femtosecond laser pulses in bulk fused silica, J. Opt. Soc. Am. B. 23 (11) (2006).
[44] S. Curran, et al., Evolution and evaluation of the polymer/nanotube composite, Synthetic Metals 101–103 (1–3) (1999) 2559.
[45] A. Valdmanis, L. Fork, Design considerations for a femtosecond pulse laser balancing self phase modulation, group velocity dispersion, saturable absorption, and saturable gain, IEEE J. Quantum Electron. 22 (1) (1986) 112–118.
[46] Kogelnik H., Bell Syst. Tech. J. 48 (1969) 2909–2947.
[47] L. Ye, et al., NUV femtosecond laser inscription of volume bragg gratings in poly(methyl)methacrylate with linear and circular polarizations, Laser Phys. 23 (12) (2013) 70.
[48] D. Liu, et al., High-speed uniform parallel 3D refractive index micro-structuring of poly(methyl methacrylate) for volume phase gratings, Appl. Phys. (2010).